REVISION 3

Controls of P-T path and element mobility on the formation of corundum pseudomorphs in Palaeoproterozoic high-pressure anorthosite from Sittampundi, Tamil Nadu, India

Priyadarshi Chowdhury,[1] Moumita Talukdar,[1] Pulak Sengupta,[1,*] Sanjoy Sanyal,[1] and D. Mukhopadhyay[2]

[1] Department of Geological Sciences, Jadavpur University, Kolkata 700032, India

[2] Department of Geology, University of Calcutta, 29, Ballygunge Circular Road, Kolkata 700019, India

*E-mail: pulaksg@gmail.com (P.Sengupta)

ABSTRACT

The Archaean Sittampundi Layered Magmatic Complex (SLC) of south India is interpreted as a part of the oceanic crust that formed in a suprasubduction zone setting. The assemblage corundum + anorthite + amphibole (magnesiohornblende to tschermakite to pargasite) + clinozoisite (C_1PACz) developed in highly calcic anorthosite of the SLC at the culmination of a c. 2.46 Ga tectonothermal event. Changing physicochemical conditions during this early Palaeoproterozoic (Siderian) event produced spinel + anorthite + second generation amphibole through destabilization of corundum + first generation amphibole. Spinel retains the shape of the corundum that it replaces (spinel pseudomorphing corundum, SCP) and is surrounded by a rind of plagioclase that separates spinel from the matrix amphibole. Development of the assemblage chlorite + clinozoisite + secondary corundum after spinel + anorthite + amphibole marks the terminal metamorphic event in this area. Mass balance calculations on pseudomorphs and modeling of preserved reaction textures show that Na, Mg, Ca and silica were mobile during the formation of the SCP. Al and Fe were mobile in grain scale but remained immobile in the scale of a thin section. Activity adjusted partial petrogenetic grid in the systems Na_2O-CaO-Al_2O_3-SiO_2-H_2O (NCASH) and Na_2O-CaO-MgO-Al_2O_3-SiO_2-H_2O (NCMASH) along with the mineralogy of the rocks that were co-metamorphosed with the anorthosite show that (a) the assemblage C_1PACz was formed during high pressure metamorphism (11 ± 1 kbar and 725 ± 25 ºC), (b) SCP and the plagioclase rind around it were formed during exhumation of these higher pressure rocks to lower pressure (7 ± 1 kbar, 675 ± 50 ºC) along steeply decompressive retrograde P-T path and (c) post decompression cooling and hydration at near isobaric condition triggered the formation of the chlorite – clinozoisite – secondary corundum assemblage (6-8 kbar, <620 ºC). The inferred P-T path is consistent with the view that the studied area that

represent Archaean oceanic crust of SSZ affinity was subducted and subsequently exhumed during the early Palaeoproterozoic orogeny.

Keywords: Sittampundi, anorthosite, corundum pseudomorph, oceanic crust, subduction zone

INTRODUCTION

Fluid-rock interactions operate in a wide range of geological environments from weathering of supracrustal rocks to metasomatism of the mantle-wedge above a subduction zone (e.g., Philpotts and Ague 2009). Disequilibrium between host-rock and percolating fluid commonly results in exchange of materials between solid and fluid that leads to significant change in host-rock composition (Dutrow et al. 1999, 2008; e.g., Philpotts and Ague 2009). At subduction zones, which are potential zones of fluid-rock interaction, the oceanic crust and the entrained sediments commonly undergo significant bulk compositional change and develop a sequence of replacement textures over a range of pressure-temperature conditions. Interpretation of these reaction textures is, therefore, likely to provide valuable insight about the subduction zone processes such as fluid circulation, mobility of elements, thermal gradient, burial and upliftment history of the subducted rocks (Berger et al. 2010). Pseudomorphs are a special replacement texture in which the product mineral retains the shape of the mineral that it replaces (reviewed in Putnis 2002). A number of experimental and theoretical studies have confirmed that the formation of pseudomorphs is caused by solution (of reactant phase) and precipitation (of product phase) mechanism at nearly constant volume (Putnis 2002, 2009; Putnis et al. 2005; Putnis and Putnis 2007; Putnis and John 2010). This property of pseudomorphs has been used to trace the behavior of elements during the formation of pseudomorphs (Hövelmann et al. 2010). Because rocks can develop pseudomorphs during prograde as well as retrograde metamorphism, pseudomorphic replacement textures also provide valuable information on metamorphic P-T path in orogenic belts (Dutrow et al. 2008).

In this communication we document pseudomorphic replacement textures (spinel pseudomorphing corundum, SCP) in anorthosite from the Archaean Sittampundi layered

magmatic complex (SLC) of South India. Mass-balance calculations and modeling of the pseudomorphs suggest that several elements including Al were mobile during the formation of the SCP. Pseudomorphs also constrain the metamorphic P-T path and thermal gradient during subduction of an Archaean oceanic crust at the dawn of the Proterozoic.

GEOLOGICAL BACKDROP

Intense geological and geochronological studies in the past two decades have revealed that the granulite terrain of south India can be broadly divided into three segments with contrasting geological history (reviewed in Braun and Kriegsman 2003; Ghosh et al. 2004; Dutta et al. 2011). The northern granulite terrain (NGT) is dominated by felsic orthogneisses with minor mafic, ultramafic rocks and metasediments that witnessed the last high-grade metamorphic event at c. 2.49-2.44 Ga (Ghosh et al. 2004; Sato et al. 2011; Mohan et al. 2012). In contrast to the NGT, the southernmost segment, the Madurai Block (MB), exposes larger amount of metasediments and is affected by high-grade metamorphism at c. 0.8-0.5 Ga (reviewed in Braun and Kriegsman 2003; Ghosh et al. 2004; Kooijman et al. 2011**)**. A roughly E-W trending curvilinear belt, which separates the NGT from the MB, exposes diverse lithological associations and carries the impressions of protracted geological history for over 2 billion years (c. 2.9-0.5 Ga, reviewed in Ghosh et al. 2004; Dutta et al. 2011). This curvilinear belt is believed to be dissected by a number of crustal scale shear zones that are collectively referred to as the Cauvery Shear System (CSS, Chetty1996), though the existence of a major transcurrent shear zone has been challenged by Mukhopadhyay et al. (2003). In the following section, the salient geological and geochronological features of this belt are described.

The oldest components of the CSS include a suite of mafic and ultramafic rocks with local anorthosite (leucogabbro according to IUGS nomenclature) and chromitite (reviewed in Bhaskar Rao et al. 1996; Ghosh et al. 2004; Dutta et al. 2011). At several places within the CSS, namely Sittampundi (SLC) and Bhavani Sagar (BLC), layered magmatic complexes are present (Subramanium 1956; Bhaskar Rao et al. 1996; Dutta et al. 2011). Banded Iron Formation (BIF) constitutes the only metasediment within the magmatic suite and is always associated with the mafic rocks (Bhaskar Rao et al. 1996; Ghosh et al.2004; Dutta et al.2011). Bhaskar Rao et al. (1996) obtained a Sm-Nd whole rock age of c. 2.9 Ga (2935 ± 60 Ma) which they interpreted to be the age of emplacement of the SLC and the BLC. This observation of Bhaskar Rao et al. (1996) has been corroborated by the subsequent study of Ghosh et

al. (2004). In a recent communication, Mohan et al. (2012) reported LA-ICP-MS U-Pb zircon age of c. 2.54 Ga (2541 ± 13 Ma) that the authors considered to be the age of emplacement of the anorthosite at Sittampundi. The reason for the time difference in the tune of 400Ma between the Sm-Nd whole rock and U-Pb zircon ages remains unclear. Nevertheless, all these studies support a late Archaean mafic magmatism in the CSS. The mafic-ultramafic-anorthosite-chromitite suite were intruded by voluminous felsic magmas of calc-alkaline nature during a narrow time span of c. 2.53-2.50 Ga (reviewed in Ghosh et al. 2004; Clark et al. 2009; Saitoh et al. 2011; Mohan et al. 2012). Rocks of the layered magmatic complexes, BIF and the invading felsic rocks underwent polydeformation and high-grade metamorphism at c. 2.49-2.44 Ga (Ghosh et al. 2004; Sato et al. 2011; Mohan et al. 2012 and the references cited therein). Important younger events in the CSS are marked by, (1) a thermal event at c. 2.0 Ga (Bhaskar Rao et al. 1996; Meissner et al. 2002), (2) deposition of shale-limestone-quartzite presumably representing shelf sediments with average provenance age of c.1.9 Ga (Meissner et al.2002), (3) emplacement of carbonatite, syenite at c. 0.7-0.8 Ga (reviewed in Upadhyay et al. 2006), (4) polyphase deformation and upper-amphibolite-facies metamorphism of the shelf sediments (~9 ± 1 kbar and 700 ± 50 °C , Meissner et al. 2002; Sengupta et al. 2009a) and the quartzofeldspathic rocks (Raith et al. 2010) at c. 0.6-0.5 Ga and (5) intrusion of voluminous granitoid /pegmatoid at c. 0.54-0.50 Ga (Ghosh et al. 2004; Brandt et al. 2003).

The Sittampundi Layered Magmatic Complex (SLC), which chiefly comprises mafic, ultramafic and anorthositic rocks with centimeter to meter thick layers of chromitite, occurs as an enclave within a suite of felsic rocks (the protolith of charnockite and enderbite and their retrograde equivalent hornblende-biotite gneiss) (Fig.1). Interpreting the field and petrological features Dutta et al. (2011) argued that the SLC represents a 'fossil oceanic crust' in an Archaean suprasubduction zone (SSZ) setting. Fractionation of hydrous high Al-basaltic magma derived from metasomatized upper mantle led to the formation of the highly calcic anorthosite of the SLC at <2 kbar. At places, mafic rocks (now mafic granulites) of the SLC are intercalated with BIF (Dutta et. al. 2011). Large porphyroblasts of garnet develop in the mafic granulites as well as in BIF (Fig.2a). Petrographic features show that the porphyroblastic garnet grains that are presumed to have developed during culmination of granulite facies metamorphism were partially to completely resorped to a symplectic intergrowth of orthopyroxene, plagioclase and amphibole (Bhaskar Rao et al.1996, our own data). BIF develop the assemblage garnet + orthopyroxene + magnetite +quartz ± clinopyroxene and show no resorption of porphyroblastic garnet (Dutta 2009). Mn-content of garnet and pyroxenes are low (Dutta 2009).Using multiple equilibria convergence technique (TWEEQU), Bhaskar Rao et al.

(1996) obtained 11-12 kbar pressure at ~650 °C using the core compositions of the porphyroblastic assemblages in the garnetiferous mafic rocks from the SLC. These authors also obtained a P-T condition of ~7 ± 1kbar and 700 ± 50 °C for the symplectitic assemblage. Sajeev et al. (2009) reported lenses of high-temperature eclogite (~20kbar, >1000°C) within the anorthosite. At several places, the anorthosite and the interlayered amphibolite develop pink (ruby) to colorless corundum crystals. Infiltration driven metamorphism of corundum-bearing anorthosite developed the assemblage högbomite + clinozoisite + magnetite + chlorite + calcite at 650 ± 50 °C and 7 ± 1kbar (Sengupta et al. 2009b).

SCP BEARING ANORTHOSITE OF THE STUDIED AREA

Mesoscopic features

Three corundum (± ruby)-bearing anorthosite (*sensu lato*) samples were chosen for the present study. In all the samples, milk-white anorthosite alternates with millimeter to decimeter thick layers that are rich in amphibole (>60-70 vol%, Fig.2b). A prominent planar fabric that is parallel to the penetrative regional foliation is defined by alignment of prismatic amphibole grains (Fig.2c). However, the random orientation of a few amphibole grains suggests that the formation of amphibole outlasted the deformation (Fig.2d). One sample shows a layer of chromitite that is stretched parallel to the planar fabric defined by amphibole (Fig.2c). Polygonal grains of anorthite (verified by petrography) impart a saccharoidal appearance to the rock. On the basis of the relative proportion of plagioclase and amphibole the anorthosite is divided into 'Domain-A' (>70 volume% of plagioclase) and 'Domain-B' (<50 volume% of plagioclase).

Colorless and pink corundum crystals (up to ~4 cm long), with euhedral to anhedral outline are embedded in the matrix, mostly within Domain-A and less commonly in Domain-B (Figs.3a-3d). Corundum grains with both hexagonal (basal/ 0001 face) as well as prismatic outline are observed in the same sample (Fig.3b), suggesting that the corundum crystals are randomly oriented within the rock volume. Some prismatic corundum crystals that cut across the

160 planar fabric of the host rock (Fig.3b). Grains of elongated corundum are boudinaged parallel to
161 their length (Figs.3c and 3d). There is extensive replacement of corundum by spinel but the
162 product spinel retains the external morphology of the host corundum grain (pseudomorphous
163 replacement). The early stage of replacement is manifested by the development of a thin rim of
164 spinel over corundum (Figs.3a-3d). Complete pseudomorphous replacement of corundum by
165 spinel marks the advanced stage of replacement (Figs.3b and 3c). At places within Domain-A,
166 broken and boudinaged grains of corundum are partially surrounded by spinel rims of varying
167 thickness (Figs.3cand 3d). The interface between the spinel and the corundum is sharp but highly
168 irregular. Coronitic spinel also extends as veins in the interior of the host corundum grain
169 (Fig.3c). The spinel is invariably surrounded by a rind of plagioclase grains that separates the
170 former corundum from amphibole in the matrix (Figs.3a and 3c). Image analyses of several thin
171 sections and observation from randomly cut and polished hand specimens show that the ratio of
172 the thickness of the plagioclase rind to that of the spinel corona ranges between 1.7 and 2.3.
173 Compared to Domain-A, Domain-B shows greater thickness of the plagioclase rind.

174

175 **Petrography**

176 Domain-A is chiefly made up of plagioclase (up to 70 vol%) with minor clinozoisite,
177 chlorite and amphibole (together constituting10-25 vol%). In contrast, amphibole (~50-60 vol%)
178 and plagioclase (~40-50 vol%) constitute the Domain-B. In both the domains, a granoblastic
179 fabric is formed by polygonal grains of amphibole (Am_{mx}) and plagioclase (Pl_{mx} ; Fig.4a). At
180 many places (only in Domain A), dimensional orientation of amphibole and clinozoisite define a
181 crude foliation parallel to the regional foliation. Large corundum grains (Crn_1) in both the

182 domains are embedded in a matrix consisting of polygonal plagioclase (Pl_{mx}) and amphibole
183 (Am_{mx}) (Fig.4b). Crn_1 is not in direct contact with amphibole and is separated from it by
184 successive coronae of green spinel (proximal to corundum) and plagioclase (Pl_m ; toward the
185 amphibole-plagioclase matrix) (Figs.4b and 4c). Where present, clinozoisite (Czo_1) does not
186 show any involvement in the spinel-plagioclase forming reaction. Hence, Czo_1 is considered to
187 be stable at this stage. The size of the plagioclase grains in the plagioclase rind (Pl_m) is distinctly
188 larger than the plagioclase grains in the matrix (Pl_{mx}) (Fig.4c). In most cases Crn_1 is partially
189 (Figs.4b and 4c) or completely pseudomorphed by spinel but in rare instances Crn_1 grains do not
190 develop spinel corona but are surrounded by a granoblastic fabric formed by Czo_1, Crn_1 and Pl_{mx}
191 (Fig.4d). Contacts among these three phases are obscured by the development of chlorite (Chl)
192 flakes. Aggregates of randomly oriented chlorite flakes and acicular clinozoisite (Czo_2) replace
193 the amphibole and the plagioclase in the matrix (Fig.4e). Locally, coronitic spinel that develops
194 over corundum is replaced by an aggregate of magnetite, corundum (Crn_2) and chlorite
195 (Fig.4f).The textural features described above are consistent with the following sequence of
196 mineral growth: Crn_1+amphibole + Czo_1+ plagioclase (matrix) to spinel + plagioclase (rind) to
197 chlorite + Czo_2 ~ Crn_2+magnetite+chlorite. Clinozoisite appears to be stable throughout the
198 evolution of the studied rock.

199 ## MINERAL CHEMISTRY

200 Detail chemical analyses of minerals were carried out in six anorthosite samples. Representative
201 mineral compositions in the pseudomorph domain are presented in Tables 1a-1d. Details of the
202 analytical procedure are presented in the Appendix. In the following section salient
203 compositional characteristics of the different minerals are described.

Amphibole

Representative amphibole analyses are presented in Table 1a. The amphibole is highly calcic (~1.6-1.9 apfu), magnesian [X_{Mg} = Mg/(Mg+ Fe^{2+}) = ~0.76-0.81, Table 1a] and aluminous (~2.3-2.7 apfu, Table 1a). Small and variable amount of Cr (up to ~0.09 apfu) and Ti (up to ~0.03 apfu) are noted in the analyzed amphibole (Table 1a). The mineral does not show any compositional zoning. In the classification of Leake et al. (2004), most of the amphibole compositions are plotted within the field of tschermakite with a few data straddling the boundary between tschermakite and magnesiohornblende. In one sample (S160), some amphibole compositions from the amphibole plagioclase matrix are rich in (Na+K) and are plotted in the field of pargasite. In all samples, there is no major difference in the compositions of amphiboles from domains A and B. However, a few amphibole grains (Am_m) that develop close to the SCP are rich in Al_2O_3 (by ~ 2 wt%) than the amphibole (Am_{mx}) present in the amphibole-plagioclase matrix (Table-1a).

Spinel

The spinel is rich in Mg [X_{Mg} = Mg/(Mg+Fe^{2+}) = ~0.53-0.68, Table 1b] but is low in Cr [up to 0.003 apfu, Cr#= 100 Cr/(Cr+Al)= up to ~0.1], Fe^{3+} [up to ~0.07 apfu, Fe^{3+}# = 100 Fe^{3+}/(Fe^{3+}+Al + Cr)=1.6-3.7], TiO_2 (~up to 0.001 apfu) and ZnO (~upto 0.002 apfu). X_{Mg} of the spinel is significantly lower than the X_{Mg} of the adjoining amphibole (0.76-0.81). Individual grains of spinel are compositionally homogeneous.

Corundum

The corundum is Al_2O_3-rich (>1.97 apfu, Table 1c) with small amount of Fe (up to 0.008 Fe^{3+} apfu) and Cr (<0.03 apfu, Table 1c). The chromium content imparts blood red color to corundum (ruby).

Plagioclase

The plagioclase is highly calcic ($An_{\geq 89}$, Table 1d) and a few analyses have nearly pure anorthite composition (An_{99}, Table 1d). All the plagioclase analyses show insignificant K. Owing to the extreme calcic nature, no significant compositional difference was noted between the plagioclase grains from different textural settings in the same sample (e.g., matrix and moat plagioclase, in domains A and B). However, the composition of the plagioclase grains varies from one sample to another.

Clinozoisite

The clinozoisite contains only 4-6 mol% pistacite molecules (~0.12-0.18 Fe^{3+} apfu) and does not show any significant compositional zoning (Table 1c).

Chlorite

The chlorite in all the three samples is highly magnesian [X_{Mg}= Mg / (Mg+Fe^{2+})= 0.83-0.84 with alumina content varying from ~2.6 to 2.9 Al apfu (Table 1d). Minor and variable amount of Ti and Cr are noted in the analyses (each up to 0.002 apfu, Table 1d).

THE SCP AND ELEMENT MOBILITY- A MASS BALANCE APPROACH

Being a product of constant volume process, pseudomorphism provides a reference frame for studying mobility of elements at least within the volume of the pseudomorph (e.g., Nijland and

Touret 2001; Hövelmann et al. 2010). In the following sections we have first discussed the principles of mass-balance approach and then its application to the SCP in the rocks of our study.

Following the composition-volume relationship algorithms of Grant (1986) and Gresens (1967) and their subsequent modifications (e.g., Philpotts and Ague 2009), change in concentration of a component 'j' in a mineral during its chemical alteration can be given as:

$$\Delta C_j = (V^f/V^o)\,(\rho^f/\rho^o)\,(C_j^f/C_j^\circ) - 1 \qquad -(1)$$

Where, ΔC_j– Change in concentration of j

C_j^f and C_j°– Final and initial concentration of 'j'

V^f and V^o– volume of the product phase spinel and original corundum grain respectively.

ρ^f and ρ^o– Density of product spinel and original corundum

For constant volume process, the equation (1) simplifies to,

$$\Delta C_j = (\rho^f/\rho^o)\,(C_j^f/C_j^\circ) - 1 \qquad -(2)$$

If 'j' behaves as an immobile component ($\Delta C_j = 0$), equation (2) further simplifies to,

$$C_j^f = (\rho^o/\rho^f)\,C_j^\circ \qquad -(3)$$

Equation 3 defines a line in C^f vs.C° space that passes through the origin and has a slope of ρ^o/ρ^f. If we consider the composition of the corundum (Crn_1) and spinel (Spl) as 'initial/unaltered' and 'final/altered' rock compositions respectively, then equation 3 can be written as,

$$C_j^{spl} = (\rho^{crn}/\rho^{spl})\,C_j^{crn} \qquad -(4)$$

Any chemical species that remains immobile during pseudomorphous replacement of corundum by spinel will be plotted on the straight line defined by Equation (4). On the other hand, chemical species that are plotted above or below the line mark gain or loss of mass, respectively, during

pseudomorphous replacement. The densities of corundum and spinel used in the calculations are 3.93g/cm^3 and 3.75g/cm^3, respectively (see Appendix). It is evident from Figure 5a that none of the major elements including aluminum falls on or close to the "mass-conserved" line defined by Equation (4). It is also evident from Figure 5a that FeO, MgO and MnO are added to (mass gain) and Al_2O_3, TiO_2 and Cr_2O_3 have moved out (mass loss) of the volume of the SCP. Employing Equation 2, we have computed the magnitude of change of concentrations of these chemical species during the formation of the SCP and the results are presented in Figure 5b**.** Figure 5b suggests that to form the SCP ~37 wt% Al_2O_3 is lost which is chiefly compensated by a gain in concentrations of MgO (~188280 wt%) and FeO (~3887wt%). Very high values of mass change for FeO and MgO are due to their very low concentrations in the reactant corundum. Concentrations of TiO_2 and Cr_2O_3 are reduced by ~94wt% and ~90wt%, respectively whereas concentration of MnO is increased by ~91wt% (Fig.5b).

The foregoing analysis, though support mobility of several elements in the volume of SCP, does not confirm if these chemical species were also mobile in the scale of a thin section. To evaluate the latter possibility we obtained balanced chemical reactions through textural modeling of the studied rock and present the results below.

TEXTURAL MODELING OF THE SCP- AN ALGEBRAIC ANALYSIS

Textural features of the anorthosite suggest that the SCP was formed at the expense of corundum and amphibole (Figs.3 and 4c-4f). Algebraic analysis of mineral compositions is a powerful tool to obtain balanced chemical reactions that explain the mineralogy and texture of the rocks formed in open or close systems (Fisher 1989; Lang et al. 2004). Singular value decomposition (SVD) is a simple but robust technique that is widely used by the geoscientists for modeling

metamorphic textures (Lang and Rice 1985; Lang et al. 2004; Sengupta et al. 2009b and the references cited therein). This technique checks linear dependencies and suggests possible reactions from a compositional matrix ***M*** of m minerals in terms of n components (Lang et al. 2004). In this study, the computer program CSpace (Torres-Roldan et al. 2000) was used to perform the matrix operation required for SVD. The chemical species whose compositions are suspected to have changed during the reactions are considered as mobile components during matrix operation. The mineral compositions that are used for the matrix analyses are indicated by asterisk mark in the compositional tables (Tables 1a-1d). For the present case, we have altogether 15 (16 if two amphiboles Am_{mx} and Am_{m} are taken) minerals and mobile species (m) that are defined by 12 system components (n). The CSpace program returns several balanced chemical reactions solving the m x n matrix. Of the probable reactions, those that satisfy the following criteria are likely to explain the formation of the SCP in the studied rocks:

a. The reactant and product phases as deduced from the textures must line on the opposite sides of the reaction(s).

b. Volume ratio of spinel: plagioclase calculated from the modeled chemical reaction would lie close to 1:2 (1:1.7 to 1:2.3 as observed from petrography).

c. The volumes of spinel and corundum in the deduced reactions must be similar. This is an essential criterion for pseudomorphism (e.g. Putnis 2002).

Modeling chemical reactions that triggered the formation of SCP requires composition of pristine amphibole. Studies have shown that composition of pristine amphibole may change significantly due to complex chemical substitutions with progress of chemical reactions involving amphibole (reviewed in Schumacher 2007). In Sittampundi anorthosite, amphibole compositions do not

marked variation between corundum-bearing and corundum- free layers. However, a few amphibole grains that develop proximal to SCP (Am_m) is slightly Al-rich compared to amphibole that develop in the amphibole plagioclase matrix (Am_{mx}). Exact reason for this compositional variation of amphibole is unclear. One possibility is that Am_m could form along with spinel and moat plagioclase (Pl_m) that separate corundum from matrix plagioclase and amphibole. In view of this, we have used both Am_{mx} and Am_m in textural modeling.

Using the aforesaid textural criteria (a-c) as filters the following reactions are obtained:

1. 218.494 Crn + 566.949 Am_{mx} + 9.508 Ti + 3.391 Mn + 113.872 Ca + 1.000 K = 85.390 Spl + 54.639 Pl + 561.593 Am_m+ 43.709 Al + 59.863 Mg + 23.477 Na + 5.360 H_2O
   ($\Delta V_{Crn-Spl}$= -0.388 %; Pl: Spl = 1:1.6; Crn: Am_{mx} = 0.04; Al_2O_3 loss = ~2.4 wt. %)

2. 130.706 Crn + 205.668 Am_{mx} + 3.088 Ti + 1.000 Mn + 59.714 Ca = 62.152 Spl + 65.242 Pl + 189.215 Am_m + 7.117 Al + 1.649 Cr + 14.071 Na + 16.454 H_2O
   ($\Delta V_{Crn-Spl}$= -0.256 %; Pl: Spl = 1:2.6; Crn: Am_{mx} = 0.06; Al_2O_3 loss = ~1 wt. %)

3. 214.286 Crn + 500.000 Am_{mx} + 8.503 Ti + 3.066 Mn + 123.086 Ca + 1.000 K + 57.731 SiO_2 (aq) = 65.534 Spl + 62.023 Pl + 500.000 Am_m + 60.536 Al + 44.067 Mg + 17.523 Na
   ($\Delta V_{Crn-Spl}$= -0.521 %; Pl: Spl = 1:2.4; Crn: Am_{mx} = 0.04; Al_2O_3 loss = ~ 3.7 wt. %)

4. 116.479 Crn + 205.697 Am_{mx} + 3.088 Ti + 1.000 Mn + 49.076 Ca = 62.021 Spl + 54.616 Pl + 189.241 Am_m + 1.450 Cr + 47.839 Mg + 14.583 Na + + 21.451 SiO_2 (aq) + 16.456 H_2O
   ($\Delta V_{Crn-Spl}$= -0.166 %; Pl: Spl = 1:2.2; Crn: Am_{mx} = 0.05; Al_2O_3 conserved)

330 Am_m and Am_{mx} represent compositions of tschermakite developed close to SCP and in the
331 matrix respectively (Table 1a).For each reaction we have calculated the difference in the
332 volumes of the reactant corundum and the product spinel ($\Delta V_{Crn\text{-}Spl}$) and volume ratio of
333 plagioclase: spinel and corundum: matrix amphibole using the molar volume data of minerals at
334 7 kbar and 700 °C (see Appendix). The justification for the chosen P-T values will be discussed
335 later. The amount of mobile aluminum (in Al_2O_3 wt%) is calculated from the measured mineral
336 compositions. Modeled chemical reactions 1-4 predict that several elements including Mg and
337 SiO_2 became mobile during the formation of the SCP. While reactions 1-3 suggest that
338 aluminum too became mobile, reaction 4 predicts Al-conserved reaction during the growth of
339 SCP. Petrological information cannot identify which of the four reactions was responsible for the
340 growth of SCP. The stoichiometry of reactions 1 - 3 suggests that only small amount of Al_2O_3
341 (~1-3.7 wt%) became mobile. In view of that it seems likely that large amount of Al_2O_3 (~37
342 wt%) that was released during the transformation of corundum to spinel was practically locked
343 in the structure of product plagioclase (that developed rind around the SCP) and in Am_m
344 (developed close to plagioclase rind).

345 ## THE SCP AS A RECORDER OF METAMORPHIC P-T PATH

346 The mineral assemblages of the corundum-bearing anorthosite are not suitable for application of
347 conventional geothermobarometry. Nevertheless, coexisting ortho- and clinopyroxenes in the
348 adjoining Mn-poor BIF that is co-metamorphosed with the SCP-bearing anorthosite provides
349 some temperature constraint (700 – 750 °C). The deduced temperature is to be treated as
350 minimum temperature during c. 2.46 Ga metamorphism as the pristine pyroxene compositions
351 might have reset during cooling. In the following section an attempt has been made to constrain
352 the physical conditions of formation of the peak metamorphic assemblage corundum (Crn_1) +

353 plagioclase (Pl_{mx}) + amphibole + clinozoisite (Czo_1) (referred to as C_1PACz) and of the
354 retrograde assemblages spinel + plagioclase + clinozoisite (SPCz) and Crn_2+ clinozoisite+
355 chlorite (C_2CzCh) that developed in the anorthosite. For this purpose, a partial petrogenetic grid
356 has been constructed in the systems Na_2O-CaO-Al_2O_3-SiO_2-H_2O (NCASH) and Na_2O-CaO-
357 MgO-Al_2O_3-SiO_2-H_2O (NCMASH) involving the minerals plagioclase, amphibole, clinozoisite,
358 kyanite, margarite, corundum, spinel, garnet, and chlorite. Most of these minerals form solid
359 solution and hence, their chemical potentials are adjusted for activities calculated from measured
360 chemical composition. As garnet did not develop in the rock, the chemical potential of pure
361 grossular was used. The computation process of the petrogenetic grid and the activity models for
362 the solid solution phases are presented in Appendix. In view of the mineralogy of the studied
363 rock, three invariant points (I_{1-3}) in the system NCMASH and one invariant point (I^*) in the
364 NCASH are considered. Additionally, one univariant reaction in the system NCASH that define
365 the lower pressure stability limit of clinozoisite (clinozoisite→grossular + anorthite + corundum
366 + H_2O) is also considered. The topology around the chosen NCMASH and NCASH invariant
367 points is presented in Figures 6a and 6b**.** Some of the reactions are not shown for clarity. The
368 reaction nets around the chosen invariant points bound P-T fields in which the assemblages
369 C_1PACz, SPCz and C_2CzCh are stabilized (Fig.6a). It is evident from Figure 6a that the peak
370 metamorphic assemblage (C_1PACz) was stabilized within the pressure-temperature range of 8-13
371 kbar and ~650-780 ºC. More restricted pressure range (~10-12 kbar) is obtained if the result of
372 two pyroxene thermometry (700-750ºC) from the co-metamorphosed BIF is superimposed on the
373 phase diagram (Fig.6a). The topological relations also suggest that reduced water activity that
374 results from dilution of H_2O by CO_2 and/or halide will displace the invariant points of Figure 6
375 to higher pressure and lower temperature. It then follows that the estimated pressure of 10-12

kbar (at 700-750 °C) should be treated as the minimum pressure estimate for the stability of the peak metamorphic assemblage C_1PACz. These P-T values overlap with the P-T values (11-12 kbar, ~650 °C) obtained by Bhaskar Rao et al. (1996) from the enclosing garnetiferous mafic-ultramafic rocks (Fig.6b). Topology of Figure 6a also constrains that the assemblage SPCz that includes the SCP was formed in the P-T range of 6-8 kbar, 625-725 ºC. Within the uncertainties of calculation, the estimated P-T value for SPCz overlaps with the P-T value obtained for the symplectitic assemblage replacing porphyroblastic garnet in the enclosing mafic-ultramafic rocks (7 ± 1 kbar, 700 ± 50 ºC, Bhaskar Rao et al.1996; our unpublished data; Fig.6b). The univariant reactions as depicted in Figure 6a further demonstrate that the assemblage C_2CzCh was formed from spinel ± amphibole- bearing assemblage at temperature ≤620 ºC and pressure 6-8kbar. This pressure-temperature range of the chlorite-bearing assemblage overlaps with the pressure-temperature values (7 ± 1 kbar, 650 ± 50 ºC) computed for the högbomite + chlorite + corundum- bearing assemblages developed in retrograded anorthosite from Sittampundi (Sengupta et al. 2009b) It is, therefore, likely that the assemblage C_2CzCh formed late due to cooling and hydration, presumably under near isobaric condition (Fig.6b). During this hydration event, rocks of the SLC resided at ~7kbar and awaited fresh tectonism that brought them close to the surface of the earth from where weathering and erosion exposed them to the present position.

DISCUSSION

It is evident from the foregoing analysis that subsequent to its formation as a part of the Archaean oceanic crust in suprasubduction zone setting (Dutta et al. 2011), the SLC underwent fluid-induced metamorphic reconstitution during c. 2.46 Ga high-grade event. At the first stage, the highly calcic anorthosite developed the assemblage C_1PACz. Estimated physical condition of metamorphism for the peak assemblage C_1PACz (11 ± 1 kbar, 725 ± 25 ºC) points to burial of

399 the 'fossil' oceanic crust (depth of formation of anorthosite <7 km, Dutta et al. 2011) to a depth
400 of ~33–40km. Mineral reaction that led to stabilization of porphyroblastic corundum in the
401 anorthosite and in the interbanded amphibolite is unclear. Features such as, (a) random
402 orientation of Crn_1 throughout the volume of the rock, and (b) absence of the assemblages with
403 kyanite + clinozoisite ± corundum and corundum + clinopyroxene speak against the idea that the
404 corundum-bearing anorthosite represents a ultra-high pressure rock (Morishita et al. 2004; Sajeev
405 et al. 2009). Desilication and decalcification of calcic plagioclase and amphibole appears to
406 explain most of the mesoscopic features of porphyroblastic corundum (e.g., Bucher et al. 2005;
407 Raith et al. 2008). Existing tectonic models suggest that burial of oceanic crust to a depth >30km
408 is only possible in subduction zones (Platt 1993; Zhang et al. 2006; Ota and Kaneko 2010; van
409 Hunen and Moyen 2012 and the references cited therein). It then follows that the SLC which was
410 a part of an Archaean suprasubduction zone was transformed to a subduction zone and buried to
411 depth of >30 km at c. 2.46 Ga. The estimated physical condition of formation of C_1PACz (~11 ±
412 1kbar and 725 ± 25ºC) corresponds to a thermal gradient of 17-22ºC/km at the time of the c. 2.46
413 Ga tectonothermal event. Such apparent thermal gradient which overlaps the domain of high
414 pressure metamorphism (≤20 °C/km) is sparsely reported from the rocks of early
415 Palaeoproterozoic age (>2.0 Ga, reviewed in Brown 2007; Anderson et al. 2012). High heat flow
416 of the ancient earth is deemed responsible for the rarity of high pressure metamorphism at the
417 dawn of the Proterozoic and earlier (reviewed in Brown 2007). Our study corroborates the
418 contention of Anderson et al. (2012) that low thermal gradient that is characteristic of the
419 orogenic belts of the Mesoproterozoic and younger time also existed in the south Indian granulite
420 belt at the dawn of Proterozoic.

In the second stage, the subducted oceanic crust that is represented by high-pressure rock of the SLC was exhumed from 11 ± 1 kbar to 7 ± 1 kbar along a steep P-T path (Figs. 6b). Infiltration-driven processes during this exhumation destabilized the porphyroblastic corundum and the amphibole and triggered the growth of the SCP with plagioclase rind. A large mismatch of crystallographic parameters exist between spinel (cubic) and corundum (hexagonal) and their textural relations are consistent with the idea that solution (of corundum)-precipitation (of spinel) process was instrumental in the formation of the SCP (Putnis 2002, 2009; Putnis et al. 2005; Putnis and Putnis 2007; Putnis and John 2010). Mass-balance calculations performed on SCP show that several chemical species including Al became mobile during the formation of SCP. However, modeling of reaction textures show that aluminum that was released during the formation of SCP was practically locked in the product minerals (plagioclase and amphibole) that develop proximal to SCP. This study therefore supports the low solubility of aluminum in metamorphic fluid.

ACKNOWLEDGEMENTS

PC, MT, PS, SS and DM acknowledge the financial support from C.S.I.R. New Delhi. SS and PS also acknowledge the financial assistance from CAS, Department of Geological Sciences, Jadavpur University and UPE (Phase II), Jadavpur University. DM acknowledges support through the Honorary Scientist Project of INSA. We are thankful to Prof. J.C. Schumacher and Prof. T. Chacko for their extremely constrictive reviews on the earlier version of this manuscript. These reviews have substantially improved the quality and clarity of the revised version. Prof. E. Ghent is thanked for his editorial comments and many helpful suggestions for the clarity of this manuscript. We thank, Dr. Uttam. K. Bhui of Pandit Deendayal Petroleum University and Dr.

Upama Dutta of University of South Florida for their valuable opinion on several aspects of this work.

REFERENCES CITED

Anderson, J. R., Payne, J.L., Kelsey, D.E., Hand, M., Collins, A. S. and Santosh, M. (2012) High-pressure granulites at the dawn of the Proterozoic.Geology, 40, 431-434.

Berger, J., Féménias, O.,Ohnenstetter, D., Plissart, G. and Mercier, J.-C.C. (2010) Origin and tectonic significance of corundum–kyanite–sapphirine amphibolites from the Variscan French Massif Central. Journal of Metamorphic Geology, 28, 341-360.

Bhaskar Rao, Y.J., Chetty, T.R.K., Janardhan, A.S. and Gopalan, K. (1996) Sm–Nd and Rb–Sr ages and *P–T* history of the Archaean Sittampundi and Bhavani layered meta-anorthosite complexes in Cauvery Shear Zone, South India: Evidence for Late Proterozoic reworking of Archean crust. Contributions to Mineralogy and Petrology, 125, 237–250.

Brandt, S., Klemd, R. and Okrusch, M. (2003) Ultrahigh-temperature metamorphism and multistage evolution of garnet–orthopyroxene granulites from the Proterozoic Epupa Complex, NW Namibia. Journal of Petrology, 44, 1121-1144.

Braun, I. and Kriegsman, L.M. (2003) Proterozoic crustal evolution of southernmost India and Sri Lanka. In M.Yoshida, B.F. Windley and S. Dasgupta, S., Eds., Proterozoic East Gondwana: Supercontinent Assembly and Breakup, 206, p. 169–202.Geological Society of London, Special Publications.

Brown, M. (2007) Metamorphic conditions in orogenic belts: A record of secular change. International Geology Review, 49, 193–234.

Bucher, K., de Capitani, C. and Grapes, R. (2005) The development of a margarite - corundum blackwall by metasomatic alteration of a slice of mica schist in ultramafic rocks, Kvesjöen, Norwegian Caledonides. Canadian Mineralogist, 43, 129-156.

Chetty, T.R.K. (1996) Proterozoic shear zones in southern granulite terrain, India. In M. Santosh and M. Yoshida, Eds., The Archaean and Proterozoic Terrains in Southern India within East Gondwana, 3, p. 77–89. Gondwana Research Group Memoir,I nternational Association for Gondwana Research, Trivandrum, India.

Clark, C., Collins, A.S., Timms, N.E., Kinny, P.D., Chetty, T.R.K. and Santosh, M. (2009) SHRIMP U–Pb age constraints on magmatism and high-grade metamorphism in the Salem Block, southern India. Gondwana Research, 16, 27–36.

Connolly, J.A.D. (2005) Computation of phase equilibria by linear programming: A tool for geodynamic modeling and its application to subduction zone decarbonation. Earth and Planetary Science Letters, 236, 524-541.

Dutrow, B.L., Foster C.T. Jr. and Whittington, J. (2008) Prograde muscovite-rich pseudomorphs as indicators of conditions during metamorphism: An example from NW Maine.American Mineralogist, 93, 300–314.

Dutrow, B.L., Foster, C.T., and Henry, D.J. (1999) Tourmaline-rich pseudomorphs in sillimanite zone metapelites; demarcation of an infiltration front. American Mineralogist, 84, 794-805.

Dutta, U. (2009) Petrology of a suite of mafic rocks and metapelites from parts of the southern granulite terrain, South India. 162-165 p., Ph.D thesis, Jadavpur University, Kolkata.

Dutta,U., Bhui, U.K., Sengupta, P., Sanyal, S. and Mukhopadhyay, D. (2011) Magmatic and metamorphic imprints in 2.9 Ga chromitites from the Sittampundi layered complex, Tamil Nadu, India. Ore Geology Reviews, 40, 90–107.

Fisher, G.W. (1989) Matrix analysis of metamorphic mineral assemblages andreactions. Contributions to Mineralogy and Petrology, 102, 69-77.

Ghosh, J.G., De Wit, M.J. and Zartman, R.E. (2004) Age and tectonic evolution of Neoproterozoic ductile shear zones in the southern granulite terrain of India with implications for Gondwana studies. Tectonics, 23, 1–38.

Grant, J.A. (1986) The isocon diagram- A simple solution to Gresens' equation for metasomatic alteration. Economic Geology, 81, 1976–1982.

Gresens, R.L. (1967) Composition–volume relationships of metasomatism. Chemical Geology, 2, 47–65.

Holland, T.J.B. and Powell, R. (1998) An internally consistent thermodynamic data set for phases of petrological interest. Journal of Metamorphic Geology, 16, 309-343.

Hövelmann, J., Putnis, A., Geisler, T., Schmidt, B.C. and Golla-Schindler, U. (2010) The replacement of plagioclase feldspars by albite: Observations from hydrothermal experiments. Contributions to Mineralogy and Petrology, 159, 43–59.

Kooijman, E., Upadhyay, D., Mezger, K., Raith, M.M., Berndt, J. and Srikantappa, C. (2011) Response of the U-Pb chronometer and trace elements in zircon to ultrahigh-temperature metamorphism: The Kadavur anorthosite complex, southern India. Chemical Geology, 290, 177-188.

Kretz, R. (1983) Symbols for rock-forming minerals. American Mineralogist, 68, 277–279.

Lang, H.M. and Rice, J. M. (1985) Regression modelling of metamorphic reactions in metapelites, Snow Peak, northern Idaho. Journal of Petrology, 26,857-887.

Lang, H.M., Watcher, A.J., Peterson, V.L., and Ryan, J.G. (2004) Coexisting clinopyroxene / spinel and amphibole/spinel symplectites in metatroctolite from the Buck Creek ultramafic body, North Carolina Blue Ridge. American Mineralogist, 89, 20–30.

Leake, B.E., Woolley, A.R., Birch, W.D., Burke, E.A.J., Ferraris, G., Grice, J.D., Hawthorne, F.C., Kisch, H.J., Krivovichev, V.G., Schumacher, J.C., Stephenson, N.C.N., and Whittaker, E.J.W. (2004) Nomenclature of amphiboles: Additions and revisions to the International Mineralogical Association's amphibole nomenclature. American Mineralogist, 89, 883-887.

Meissner, B., Deters, P., Srikantappa, C. and Kohler, H. (2002) Geological evolution of the Moyer, Bhavani and Palghat shear zones of southern India: Implications for Gondwana correlation. Precambrian Research, 114, 149–175.

Mohan, M.R., Satyanarayanan, M., Santosh, M., Sylvester, P. J., Tubrett, M. and Lam, R. (2012) Neoarchean suprasubduction zone arc magmatism in southern India: Geochemistry, zircon U-Pb geochronology and Hf isotopes of the Sittampundi Anorthosite Complex. Gondwana Research, in press, DOI:10.1016/j.gr.2012.04.004.

Morishita, T., Arai, S. and Green, D. H. (2004) Possible non-melted remnants of subducted lithosphere: Experimental and geochemical evidence from corundum-bearing mafic rocks in the Horoman peridotite complex, Japan. Journal of Petrology, 45, 235–252.

Mukhopadhyay, D., Senthil kumar, P., Srinivasan, R. and Bhattacharyya, T. (2003) Nature of the Palghat-Cauvery lineament in the region south of Namakkal, Tamilnadu: Implications for the terrane assembly in the south Indian granulite province. Memoir, Geol. Soc. India, 50, 279-296.

Nijland, T. G. and Touret, J. L. R. (2001) Replacement of graphic pegmatite by graphic albite-actinolite-clinopyroxene intergrowths (Mjåvatn, southern Norway). European Journal of Mineralogy.13, 41-50.

Ota, T. and Kaneko, Y. (2010) Blueschists, eclogites, and subduction zone tectonics: Insights from a review of Late Miocene blueschists and eclogites, and related young high-pressure metamorphic rocks. Gondwana Research, 18, 167–188.

Philpotts, A. and Ague, J. (2009) Principles of igneous and metamorphic petrology, Eds.2. Cambridge University Press, Cambridge, UK.

Platt, J.P. (1993) Exhumation of high-pressure rocks: A review of concepts and processes. Terra Nova, 5, 119–133.

Putnis, A. (2002) Mineral replacement reactions: from macroscopic observations to microscopic mechanisms. Mineralogical Magazine, 66, 689-708.

Putnis, A. (2009) Mineral Replacement Reactions. In E.H. Oelkers and J. Schott, Eds., Thermodynamics and Kinetics of Water-Rock Interaction, 70, p. 87-124.Reviews in Mineralogy

and Geochemistry, Mineralogical Society of America and The Geochemical Society, Chantilly, Virginia.

Putnis, A. and John, T. (2010) Replacement processes in the Earth's crust. Elements, 6, 159-164.

Putnis, A. and Putnis, C. V. (2007) The Mechanism of reequilibration of solids in the presence of a fluid phase. Journal of Solid State Chemistry, 180, 1783-1786.

Putnis, C. V., Tsukamoto, K. and Nishimura, Y. (2005) Direct observations of pseudomorphism: Compositional and textural evolution at a fluid-solid interface. American Mineralogist, 90, 1909-1912.

Raith, M.M., Rakotondrazafy, R. and Sengupta, P. (2008) Petrology of corundum-spinel-sapphirine-anorthite rocks (sakenites) from the type locality in southern Madagascar. Journal of Metamorphic Geology, 26, 647–667.

Raith, M.M., Srikantappa, C., Sengupta, P., Kooijman, E. and Upadhyay, D. (2010) Corundum–leucosome-bearing aluminous gneiss from Ayyarmalai, Southern Granulite Terrain, India: A textbook example of vapor phase-absent muscovite-melting in silica undersaturated aluminous rocks. American Mineralogist, 95, 897–907.

Saitoh, Y., Tsunogae, T., Santosh, M., Chetty, T.R.K. and Horie, K. (2011) Neoarchean high pressure metamorphism from the northern margin of the Palghat-Cauvery suture zone, southern India: Petrology and zircon SHRIMP geochronology. Journal of Asian Earth Sciences, 42, 268–285.

562 Sajeev, K., Windley, B.F., Connolly, J.A.D. and Kon, Y. (2009) Retrogressed eclogite (20 kbar,
563 1020 °C) from the Neoproterozoic Palghat-Cauvery suture zone, southern India. Precambrian
564 Research, 171, 23–36.

565 Sato, K., Santosh, M., Tsunogae, T., Chetty, T.R.K. and Hirata, T. (2011) Laser- ablation ICP
566 mass spectrometry for zircon U–Pb geochronology of metamorphosed granite from the Salem
567 Block: implication for Neoarchean crustal evolution in southern India. Journal of Mineralogical
568 and Petrological Sciences, 106, 1-12.

569 Schumacher, J. C. (2007) Metamorphic amphiboles: composition and coexistence. Reviews in
570 Mineralogy and Geochemistry, 67, 359-416.

571 Sengupta, N., Sengupta, P. and Sachan, H. (2011) Aluminous and alkali-deficient tourmaline
572 from the Singhbhum Shear Zone, East Indian Shield: Insight for polyphase boron infiltration
573 during regional metamorphism. American Mineralogist, 96, 752-767.

574 Sengupta, P., Bhui, U.K., Braun, I., Dutta, U. and Mukhopadhyay, D. (2009b) Chemical
575 substitutions, paragenetic relations and physical conditions of högbomite in Sittampundi layered
576 anorthosite complex, south India. American Mineralogist, 94, 1520–1534.

577 Sengupta, P., Dutta, U., Bhui, U. and Mukhopadhyay, D. (2009a) Genesis of wollastonite- and
578 grandite-rich skarns in a suite of marble–calc–silicate rocks from Sittampundi, Tamil Nadu:
579 Constraints on the P–T–fluid regime in parts of the Pan-African mobile belt of South India.
580 Mineralogy and Petrology, 95, 179–200.

581 Subramanium, A.P. (1956) Mineralogy and petrology of the Sittampundi complex, Salem
582 district, Madras State, India. Geological Society of America Bulletin, 67, 317–390.

583 Torres-Roldan, R.L., Garcia-Casco, A., and Garcia-Sanchez, P.A. (2000) C-Space: An integrated
584 workplace for the graphical and algebraic analysis of phase assemblages on 32-bit wintel
585 platforms. Computers and Geosciences, 26, 779-793.

586 Upadhyay, D., Jahn-Awe, S., Pin, C., Paquette, J.L. and Braun, I. (2006) Neoproterozoic alkaline
587 magmatism at Sivamalai, Southern India. Gondwana Research, 10, 156–166.

588 Van Hunen, J. and Moyen, J.F. (2012) Archean Subduction: Fact or Fiction? Annual Review of
589 Earth and Planetary Sciences, 40, 195-219.

590 Zhang, J., Zhao, G., Sun, M., Wilde, S.A., Li, S. and Liu, S. (2006) High-pressure mafic
591 granulites in the Trans-North China Orogen: Tectonic significance and age. Gondwana Research,
592 9, 349–362.

593 ## LIST OF FIGURE CAPTIONS

594 **Figure 1.** Generalized geological map of Cauvery Shear System (CSS; Chetty, 1996) (modified
595 after the geological map of Tamil Nadu, 1: 250 000 scale, published by the Geological Survey of
596 India 1995). The studied area is marked by a square in the inset. Various shear zones in CSS and
597 adjoining areas are shown in the inset. DC- Dharwar Craton, FL- Fermore line separating
598 northern DC from the Southern India Granulite Terrane, NGT- Northern Granulite Terrane,
599 MSZ- Moyar shear zone, BSZ- Bhavani shear zone, MBASZ- Moyar-Bhavani-Attur shear zone,
600 PCSZ- Palghat– Cauvery shear zone, MB- Madurai Block, KKPTSZ- Karur–Kumbum–Panivu–
601 Trichur shear zone (Ghosh et al., 2004), ACSZ- Achankovil shear zone, KKB- Kerala khondalite
602 belt, BLC- Bhavani layered complex, SLC- Sittampundi layered complex.

603

604 **Figure 2. (a)-** Dismembered band of clinopyroxenite dykes (dark) within anorthosite (white).
605 Note the large porphyroblastic garnet (Grt) grains in the clinopyroxenite dyke. **(b)-** Amphibole
606 (Am) rich layers (dark) within anorthosite (white). **(c)-** Dimensional orientation of amphibole
607 (Am) grains defining the foliation within anorthosite. In the middle of the slab a cm-thick
608 chromite (Chr) layer is present within the anorthosite. Note that the chromite (Chr) layer is
609 stretched parallel to the foliation defined by amphibole (Am). Pink corundum (Crn_1) with a rim
610 of spinel is seen within anorthosite in the lower part of the slab. **(d)-** Haphazard orientation of
611 large amphibole (Am) grains within anorthosite (white). The Mineral abbreviations are after
612 Kretz et al. (1983).

613

614 **Figure 3. (a)-** Large corundum (Crn_1) with hexagonal outline is embedded within amphibole rich
615 (dark) domain within anorthosite. Note that Spinel (Spl) that rims Crn_1 also retains the hexagonal
616 shape of the original Crn_1 (pseudomorph). Also note that a rind of plagioclase (Pl_m) separates Spl
617 from matrix amphibole (Am_{mx}) + plagioclase (Pl_{mx}). Domain-B. See text. **(b)-** Prismatic Crn_1
618 (ruby) cuts the foliation defined by Am (dark green) in Domain-B. In Domain-A (lower half)
619 Crn_1 shows oval to hexagonal outline. These features are consistent with haphazard orientation
620 of Crn_1 in the rock volume. Spl rim on Crn_1 grains are also seen. Note that some Crn_1 grains are
621 completely pseudomorphed by Spl. See text. **(c)-** Development of coarse Crn_1 in Am-Pl_{mx}
622 matrix. Crn_1 develops Spl rims of variable thickness. Spl retains the shape of Crn_1 and is
623 surrounded by Pl_m near Am. Coronal Spl send vein towards the interior and fill fractures within
624 the Crn_1 grains. See text. Complete pseudomorphic replacement of Crn_1 by Spl is also seen. The
625 mineral abbreviations are after Kretz et al. (1983). **(d)-**Boudinaged prismatic Crn_1 (ruby) crystal

626 partially replaced by Spl within plagioclase rich domain (Domain-A). Note that Spl retains the
627 shape of the Crn_1boudins. Patches of amphibole (Am_m) are seen close to the Crn_1-Spl domain.

628

629 **Figure 4. (a)-** Granoblastic fabric defined by polygonal grains of plagioclase (Pl_{mx}) and
630 amphibole (Am_{mx}) grains in the matrix of anorthosite. Plane polarized light. **(b)-** Partial
631 replacement of Crn_1 by Spl. Note the development of Pl_m around Spl. Plane polarized light.**(c)-**
632 Same as Fig.(b) note that grains of Pl_m has larger size than that of Pl_{mx}. Domain-B, anorthosite.
633 Plane polarised light .**(d)-** Granoblastic texture shown by corundum (Crn_1), plagioclase (Pl_{mx})
634 and clinozoisite (Czo_1). Note the development of haphazard chlorite (Chl) flakes along the
635 contacts of the porphyroblastic phases. Crossed nicols. **(e)-** Aggregate of clinozoisite (Czo_2) +
636 chlorite (Chl) separate Pl_{mx} and amphibole (Am_{mx}). Domain-A. Crossed nicols. **(f)-** Breakdown
637 of coronitic Spl by into an aggregate of corundum (Crn_2; black) + magnetite (Mag; bright) +
638 chlorite (Chl; flaky) against plagioclase rind (Pl_m). Domain-A. BSE image. The abbreviations for
639 phases are same as in Figure 2 and 3 (after Kretz et al. 1983).

640

641 **Figure 5. (a)-** C_j^{spl} vs. C_j^{crn} diagram demonstrating the gains and losses of different elements
642 during the formation of spinel with corundum pseudomorphs (SCP). Initial concentration of
643 various species in corundum (C_j^{crn}) is plotted against the final concentration in spinel (C_j^{spl}).
644 Elements whose concentrations remain conserved should be plotted on the 'mass-conserved' line
645 having slope given by (ρ^{crn}/ρ^{spl}). See Equation 4 in the text. Species plotting above or below
646 'mass-conserved' Line infer mass gain or loss during the formation of SCP. Note that the

formation of SCP was accompanied by the loss of Al_2O_3, Cr_2O_3 and TiO_2 which in turn is compensated by the gain of MgO, FeO and MnO. **(b)-** Percentages of mass change undergone by individual species during the formation of SCP. Species having negative values indicate mass loss while those having positive values indicate mass gain. The extremely high positive values for FeO and MgO (plots outside the shown scale) are related to the low concentration of these species in corundum.

Figure 6. (a) Activity adjusted partial petrogenetic grid in the system Na_2O-CaO-Al_2O_3-SiO_2-H_2O (NCASH) and Na_2O-CaO-MgO-Al_2O_3-SiO_2-H_2O (NCMASH) involving the minerals those are relevant to this study. P-T stability fields of the peak assemblage Crn_1+Pl+Am+Czo_1 (C_1PACz) and retrograded assemblages Spl+Pl+Czo (SPCz) and Crn_2+Czo+Chl (C_2CzCh) of the studied anorthosite are shaded. Lines marked (a) and (b) represent the temperature range estimated from the enclosing BIF. $I_{1\text{-}3}$ and I* are the invariant points in the NCMASH and NCASH systems respectively. **(b)** Metamorphic P-T path deduced from the SCP-bearing anorthosite. 'x' and 'y' represent the P-T ranges for the peak and retrograde assemblages as obtained from the mafic granulites by Bhaskar Rao et al. 1996 (see text). The bold and dashed line with an arrow head represents the probable P-T path traversed by the studied rock. Some of the reaction lines and labels are omitted for clarity. The abbreviations for phases are after Kretz et al. (1983).

APPENDIX

Mineral abbreviation

668 The mineral name abbreviations used here are after Kretz et al. 1983. Amphibole is
669 abbreviated as 'Am'. Subscript 'm' and 'mx'are used after mineral abbreviation (Am and Pl) to
670 indicate the presence of the phase near or within SCP and within matrix respectively. Different
671 generations of the same mineral is denoted by mentioning '1' or '2' for first or second generation
672 respectively in the subscript of the mineral abbreviation e.g., Crn_1 and Crn_2.

673 **Microprobe analysis**

674 Representative compositions of the minerals in the pseudomorph forming domains were
675 measured with CAMECA-SX 100 at Geological Survey of India, Kolkata. Analyses were carried
676 out with an electron beam (1-2μm diameter) operated at 15kv and 15 nA. Details of the
677 analytical procedure and the standard used for analyses are given in Sengupta et al. (2011).

678 **Activity-composition relations used for Figure 6**

679 For construction of activity adjusted topologies in the system Na_2O-CaO-MgO-Al_2O_3-
680 SiO_2-H_2O (NCMASH) and Na_2O-CaO-Al_2O_3-SiO_2-H_2O (NCASH), A-X program of Holland
681 and Powell (2001) is used.

682 **Molar volumes and densities of minerals**

683 The molar volume (V) and density (ρ) of the minerals that are used in this study are
684 calculated at 7 kbar, 700 °C, the mean pressure-temperature estimated for the SCP. The
685 thermodynamic data of Holland and Powell (1998 updated in 2002) and the computer program of
686 PERPLEX (Connolly, 2005) are used to obtain the molar volume and density data.

Phases	Crn	Spl	Pl(An)	Am(Ts)

V*(J/mol/bar)*	2.593	4.060	10.106	27.094
ρ*(g/cm^3)*	3.93	3.75		

For spinel, which is essentially a solid solution of $MgAl_2O_4$ and $FeAl_2O_4$ (Table 1b), molar volume and density is calculated by the relation –

$$V_{spinel} = [(X_{MgAl2O4} \times V^{MgAl2O4}) + (X_{FeAl2O4} \times V^{FeAl2O4})]$$

$$\rho_{spinel} = [(X_{MgAl2O4} \times \rho^{MgAl2O4}) + (X_{FeAl2O4} \times \rho^{FeAl2O4})]$$

where, $X_{FeAl2O4}$ represents molar mole fraction of $FeAl_2O_4$ etc. The values of the used inputs in the above calculation are - $X_{MgAl2O4} = 0.68$; $X_{FeAl2O4} = 0.32$; $V^{MgAl2O4} = 4.030$ g/cm^3; $V^{FeAl2O4} = 4.124$ g/cm^3; $\rho^{MgAl2O4} = 3.53$ g/cm^3 ; $\rho^{FeAl2O4} = 4.215$ g/cm^3.

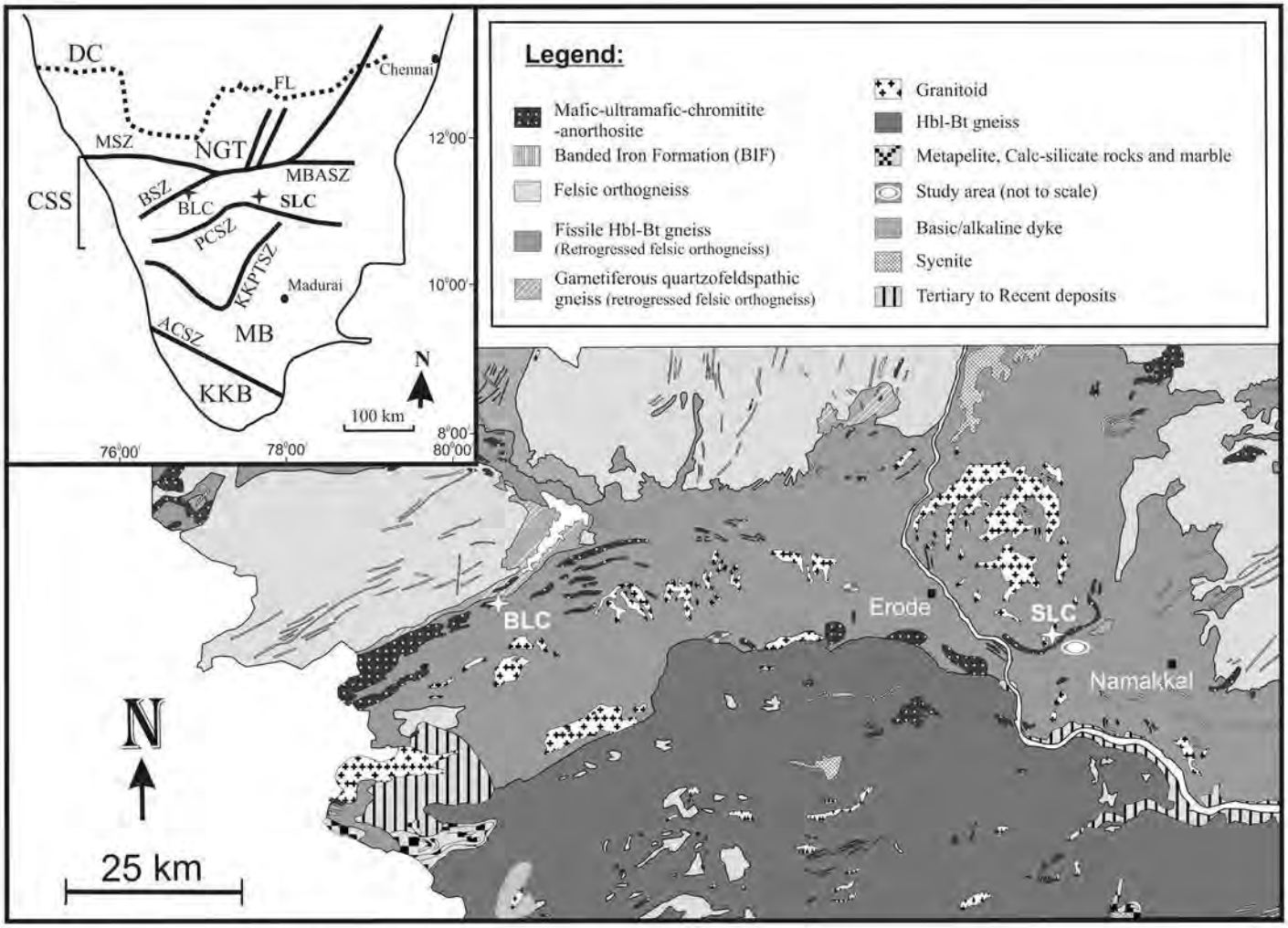
DC
FL
Chennai
MSZ
NGT
MBASZ
CSS
BSZ
BLC
SLC
PCSZ
KKPTSZ
Madurai
ACSZ
MB
KKB
N
100 km
12°00
10°00
8°00
76°00
78°00
80°00
Legend:
Mafic-ultramafic-chromitite -anorthosite
Banded Iron Formation (BIF)
Felsic orthogneiss
Fissile Hbl-Bt gneiss (Retrogressed felsic orthogneiss)
Garnetiferous quartzofeldspathic gneiss (retrogressed felsic orthogneiss)
Granitoid
Hbl-Bt gneiss
Metapelite, Calc-silicate rocks and marble
Study area (not to scale)
Basic/alkaline dyke
Sycnite
Tertiary to Recent deposits
BLC
Erode
SLC
Namakkal
N
25 km

Figure 1

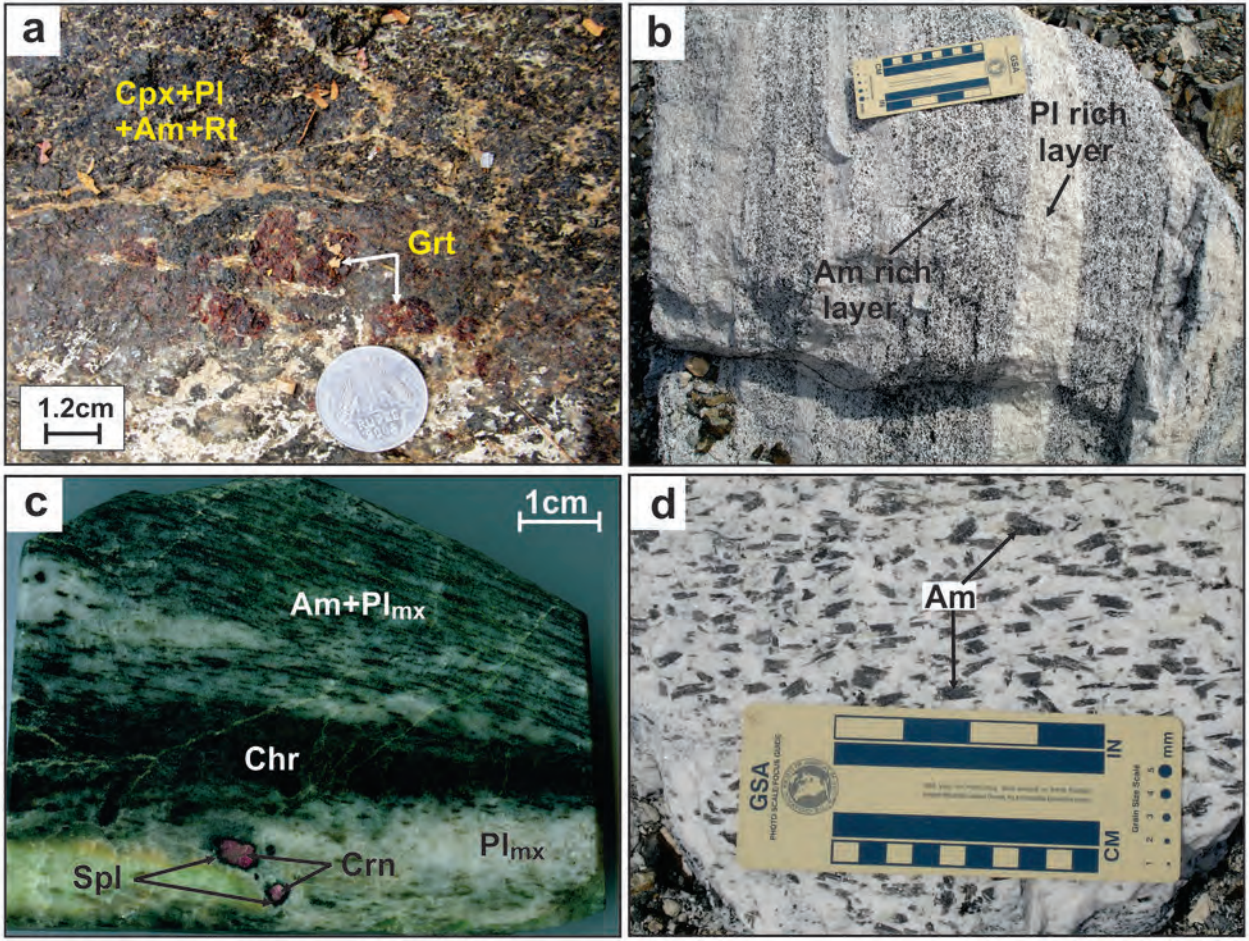
a
Cpx+Pl
+Am+Rt
Grt
1.2cm
b
Pl rich
layer
Am rich
layer
c
1cm
Am+Plmx
Chr
Plmx
Spl
Crn
d
Am
GSA
IN
CM
mm

Figure 2

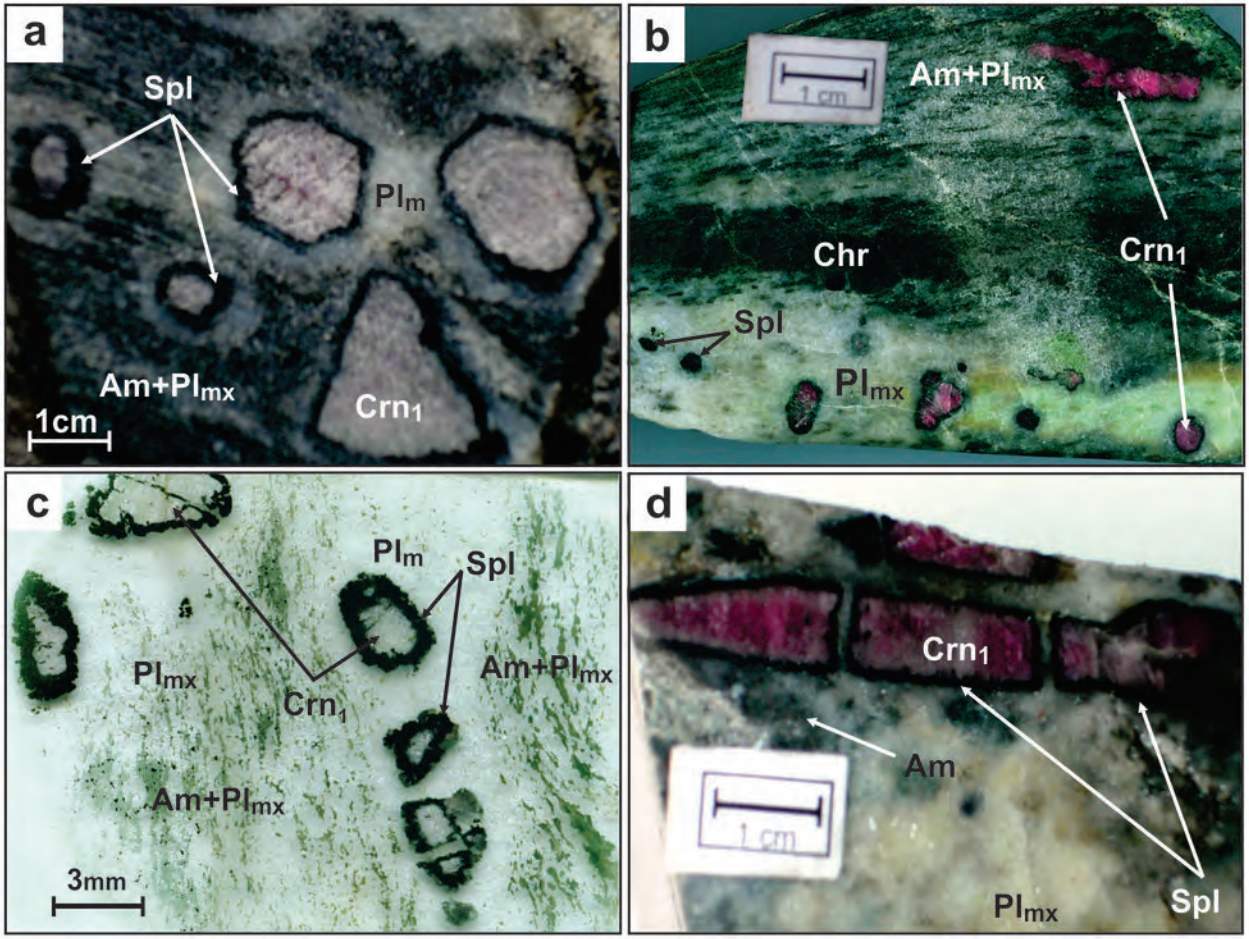
a
Spl
Plm
Am+Plmx
Crn1
1cm
b
1 cm
Am+Plmx
Chr
Crn1
Spl
Plmx
c
Plm
Spl
Plmx
Crn1
Am+Plmx
Am+Plmx
3mm
d
Crn1
Am
1 cm
Plmx
Spl

Figure 3

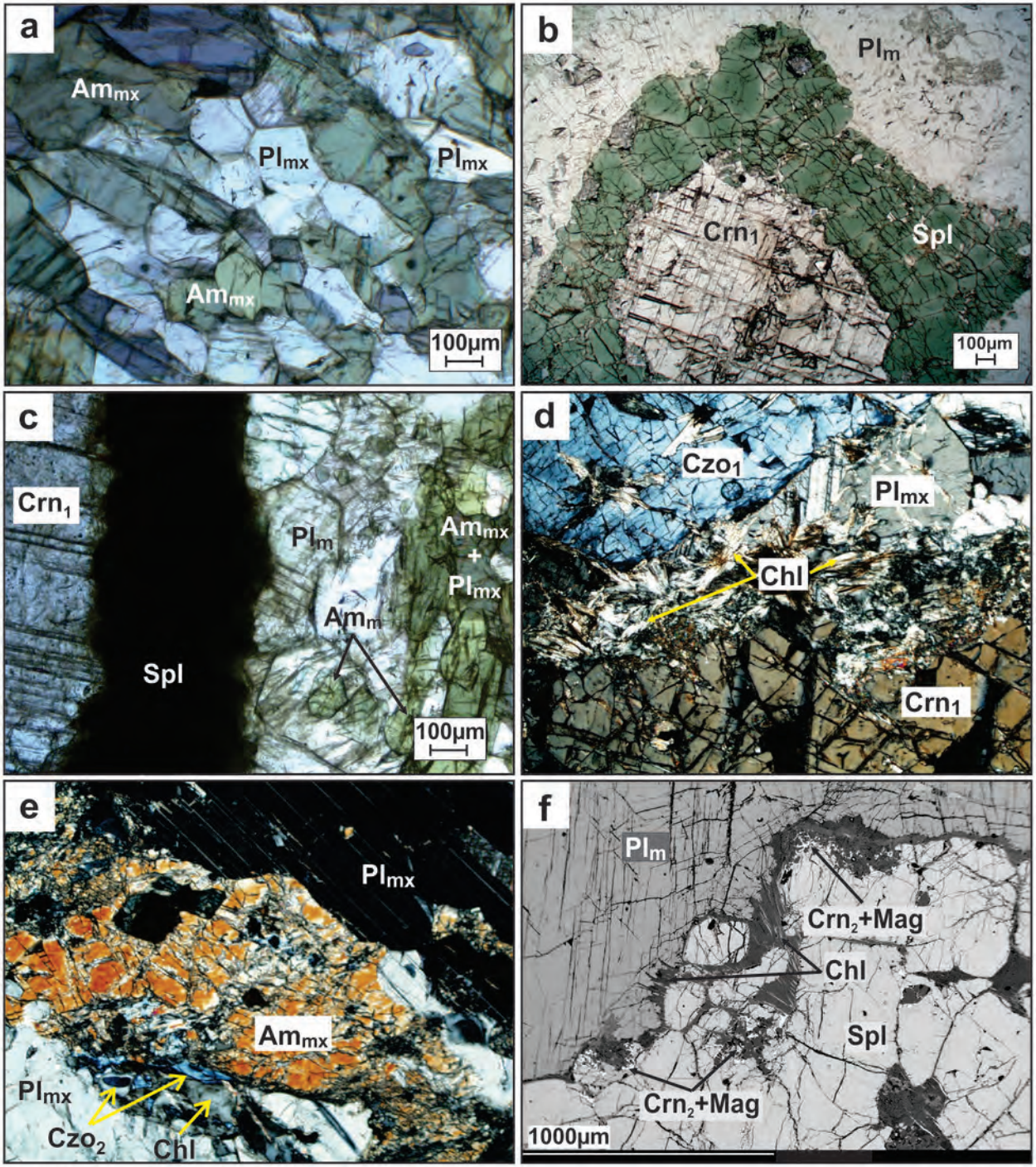
a
Am$_{mx}$
Pl$_{mx}$
Pl$_{mx}$
Am$_{mx}$
100µm
b
Pl$_m$
Crn$_1$
Spl
100µm
c
Crn$_1$
Pl$_m$
Am$_{mx}$ + Pl$_{mx}$
Am$_m$
Spl
100µm
d
Czo$_1$
Pl$_{mx}$
Chl
Crn$_1$
e
Pl$_{mx}$
Am$_{mx}$
Pl$_{mx}$
Czo$_2$
Chl
f
Pl$_m$
Crn$_2$+Mag
Chl
Spl
Crn$_2$+Mag
1000µm

Figure 4a-4f

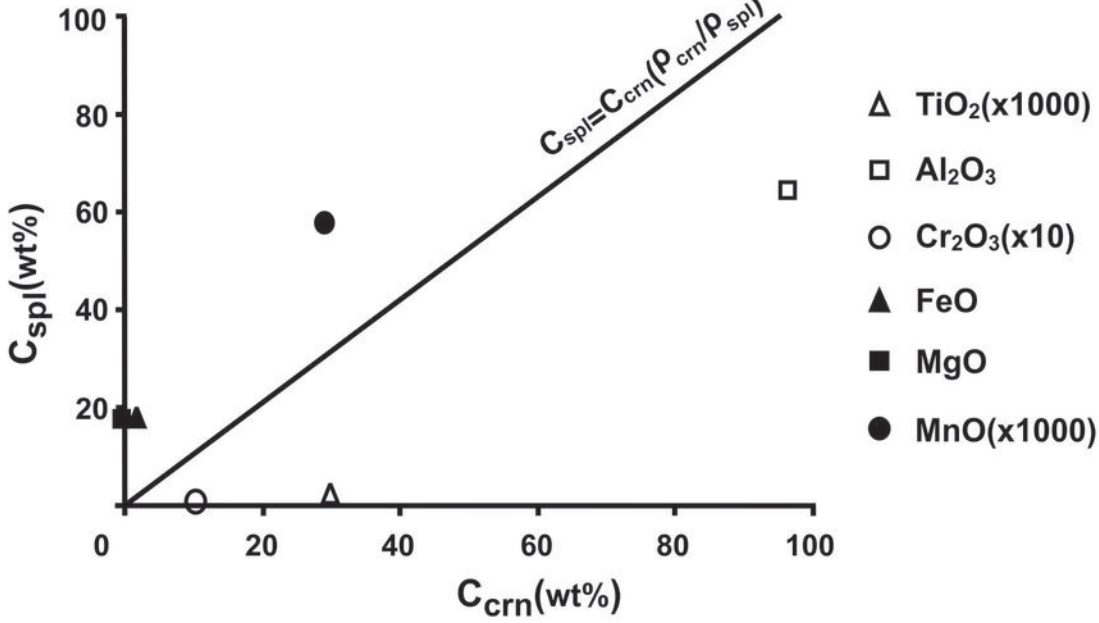
100
80
60
40
20
0
20
40
60
80
100
$C_{spl}(wt\%)$
$C_{crn}(wt\%)$
$C_{spl}=C_{crn}(\rho_{crn}/\rho_{spl})$
TiO_2(x1000)
Al_2O_3
Cr_2O_3(x10)
FeO
MgO
MnO(x1000)

Figure 5a

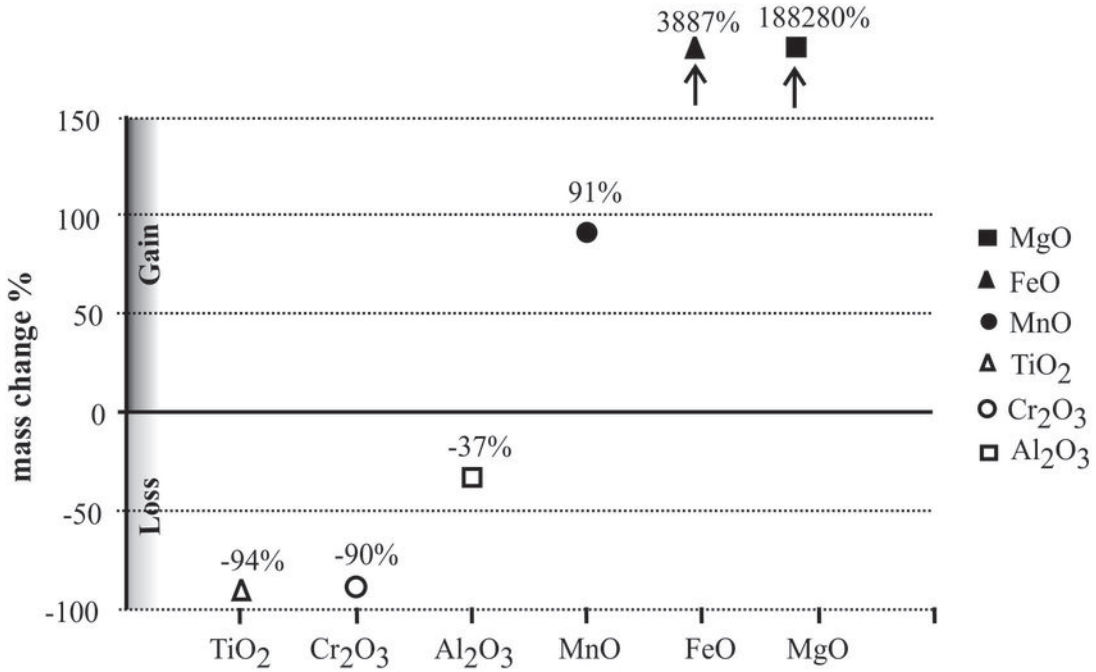
3887%
188280%
150
100
50
0
-50
-100
mass change %
Gain
Loss
91%
-37%
-94%
-90%
MgO
FeO
MnO
TiO2
Cr2O3
Al2O3
TiO2
Cr2O3
Al2O3
MnO
FeO
MgO

Figure 5b

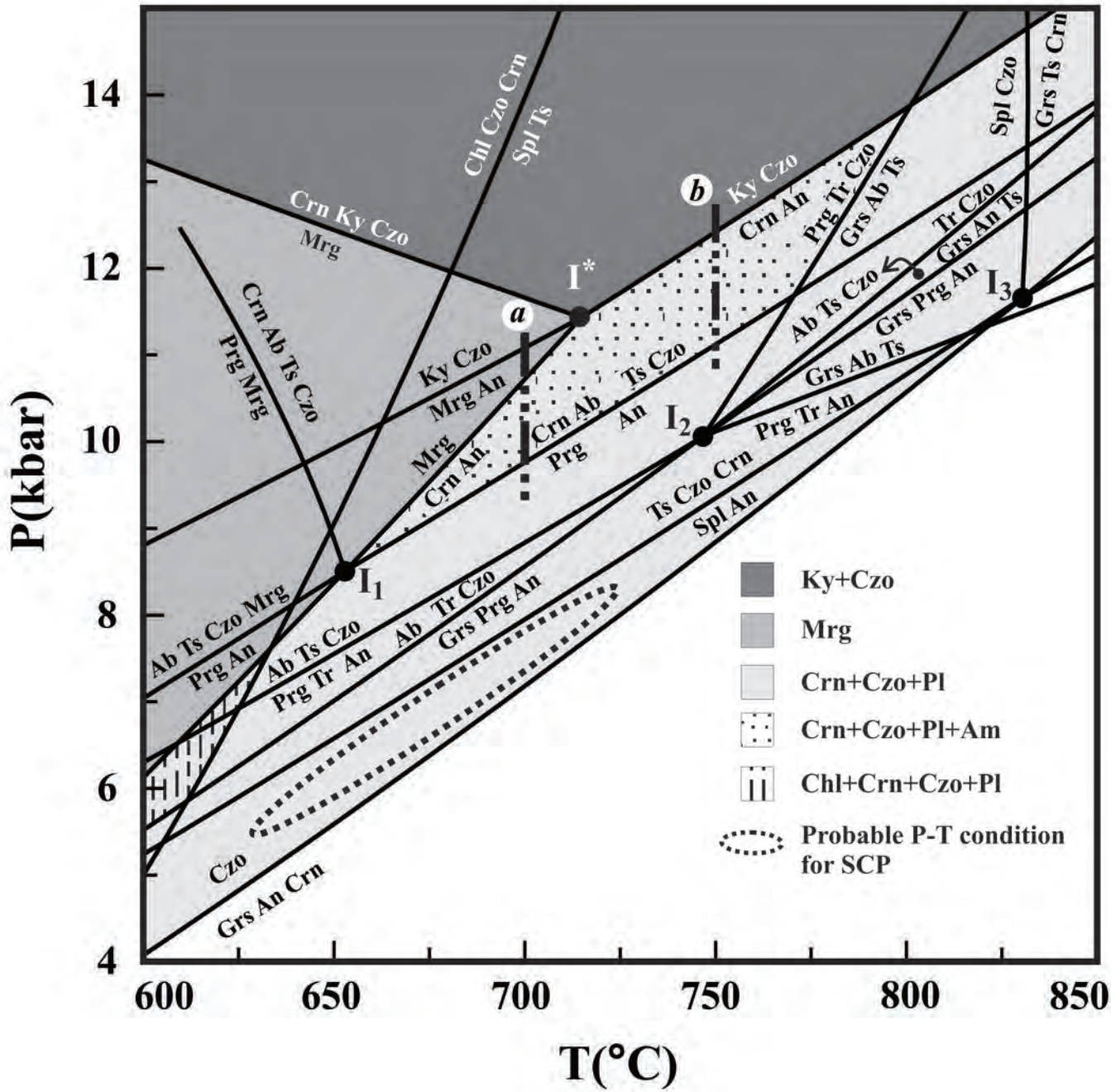
P(kbar)
T(°C)
14
12
10
8
6
4
600
650
700
750
800
850
Chl Czo Crn
Spl Ts
Crn Ky Czo
Mrg
Crn Ab Ts Czo
Prg Mrg
Ky Czo
Mrg An
Mrg
Crn An
Crn Ab
Prg
An
Ts Czo
Ab Ts Czo Mrg
Prg An
Ab Ts Czo
Prg Tr An
Ab Tr Czo
Grs Prg An
Czo
Grs An Crn
Ky Czo
Crn An
Prg Tr Czo
Grs Ab Ts
Spl Czo
Grs Ts Crn
Tr Czo
Grs An Ts
Ab Ts Czo
Grs Prg An
Grs Ab Ts
Prg Tr An
Ts Czo Crn
Spl An
I*
I1
I2
I3
a
b
Ky+Czo
Mrg
Crn+Czo+Pl
Crn+Czo+Pl+Am
Chl+Crn+Czo+Pl
Probable P-T condition for SCP

Figure 6a

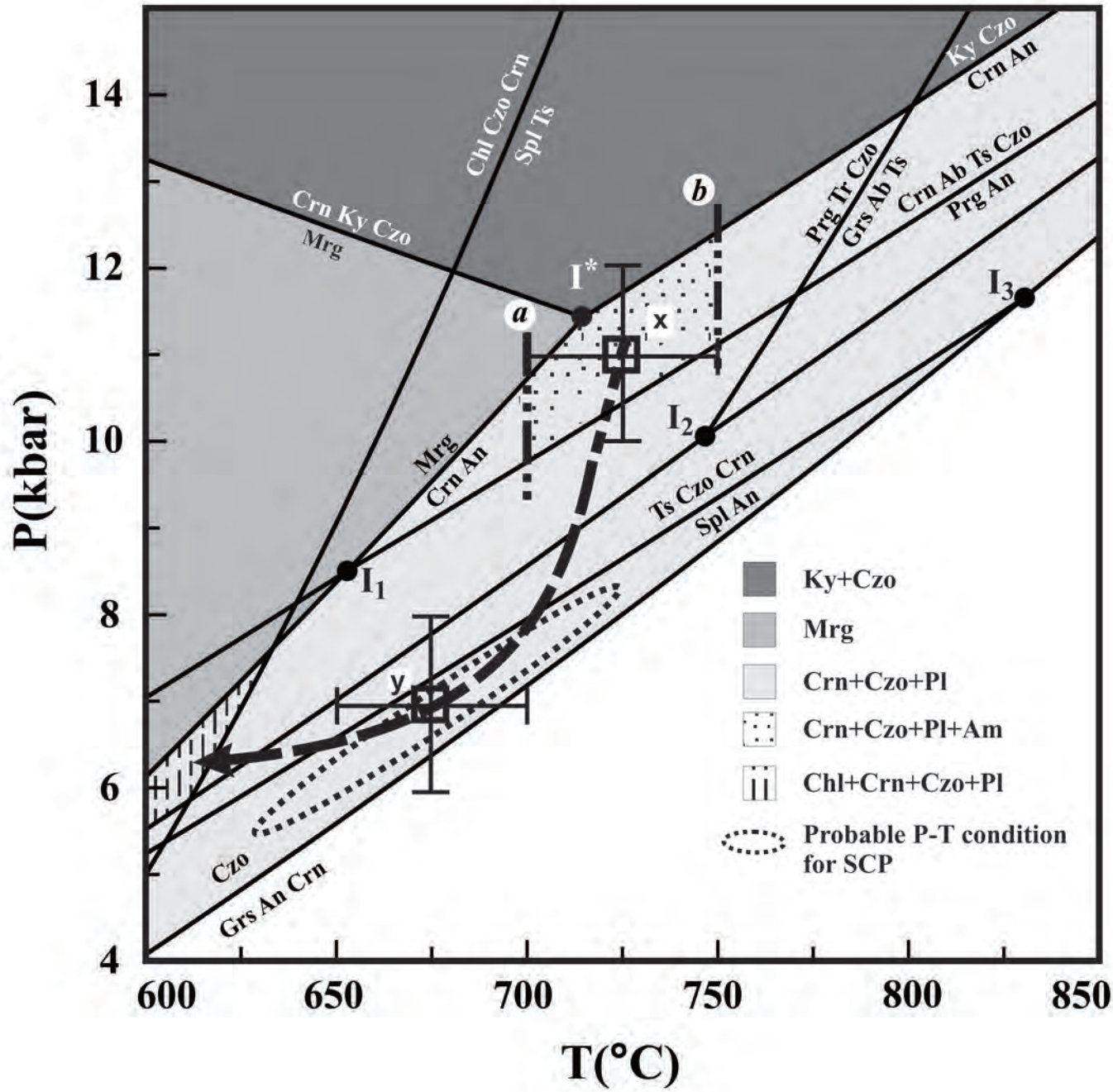
Ky Czo
Crn An
Chl Czo Crn
Spl Ts
Crn Ky Czo
Mrg
Prg Tr Czo
Grs Ab Ts
Crn Ab Ts Czo
Prg An
b
I*
a
x
I3
I2
Mrg
Crn An
Ts Czo Crn
Spl An
I1
y
Ky+Czo
Mrg
Crn+Czo+Pl
Crn+Czo+Pl+Am
Chl+Crn+Czo+Pl
Probable P-T condition for SCP
Czo
Grs An Crn
P(kbar)
T(°C)
14
12
10
8
6
4
600
650
700
750
800
850

Figure 6b

Table 1a. Representative microprobe analyses of amphibole.

Sample	S135-83	S135-84	S135-102	S140-100	S160-28*	S160-62	S160-231
SiO_2	45.75	46.29	45.27	45.24	43.40	43.83	44.35
TiO_2	0.04	0.08	0.21	0.21	0.23	0.16	0.10
Al_2O_3	13.96	13.78	13.21	15.21	15.53	15.31	14.53
Cr_2O_3	0.13	0.11	0.78	0.02	0.56	0.26	0.47
MgO	15.69	15.42	15.85	15.91	14.98	15.68	15.69
FeO	8.47	8.52	6.76	6.96	6.66	6.82	7.15
CaO	10.92	11.17	11.24	11.57	11.95	11.33	11.07
MnO	0.13	0.10	0.12	0.09	0.15	0.11	0.10
Na_2O	1.99	2.04	2.02	2.19	1.89	2.24	2.13
K_2O	0.13	0.13	0.14	0.06	0.13	0.10	0.06
Total	97.22	97.64	95.60	97.46	95.48	95.84	95.65
Cations based on 23 oxygens							
Si	6.549	6.595	6.565	6.427	6.318	6.348	6.435
Ti	0.005	0.009	0.023	0.022	0.025	0.017	0.011
Al	2.355	2.315	2.258	2.548	2.664	2.613	2.485
Cr	0.015	0.013	0.089	0.002	0.064	0.029	0.054
Mg	3.347	3.275	3.426	3.370	3.250	3.384	3.394
Fe	1.014	1.016	0.820	0.826	0.811	0.826	0.867
Ca	1.674	1.706	1.746	1.761	1.865	1.758	1.722
Mn	0.016	0.012	0.015	0.011	0.018	0.014	0.012
Na	0.552	0.563	0.568	0.603	0.533	0.628	0.600
K	0.023	0.023	0.026	0.012	0.025	0.019	0.012
Cation Σ	15.550	15.525	15.536	15.583	15.572	15.637	15.591
X_{Mg}	0.77	0.76	0.81	0.80	0.80	0.80	0.80
Species**	Tsch	MH	MH	Tsch	$Tsch_m$	$Parg_m$	$Tsch_{mx}$

X_{Mg} = Mg / ($Mg+Fe^{2+}$) ; Tsch- Tschermakite, MH- Magnesiohornblende, Parg- Pargasite

* Analyses used for reaction modeling (m= amphibole near SCP; mx= matrix amphibole, see text)

**Amphibole species nomenclature is after Leake et. al. (2004).

S160-234	S160-243*
44.39	43.83
0.11	0.08
14.71	14.02
0.47	0.50
16.13	15.62
7.19	6.98
11.32	11.05
0.08	0.10
2.20	2.01
0.11	0.12
96.71	94.31
6.383	6.453
0.012	0.008
2.493	2.433
0.053	0.058
3.456	3.427
0.865	0.859
1.744	1.743
0.010	0.012
0.613	0.574
0.020	0.023
15.649	15.591
0.80	0.80
$Tsch_{mx}$	$Tsch_{mx}$

Table 1b. Representative microprobe analyses of spinel (Spl).

Sample	S135-7	S135-16	S140-149	S160-2	S160-3	S160-16*
SiO_2	0.00	0.02	0.03	0.02	0.00	0.00
TiO_2	0.00	0.00	0.04	0.00	0.00	0.00
Al_2O_3	61.57	61.48	62.92	64.62	65.13	64.14
Cr_2O_3	0.02	0.00	0.05	0.12	0.08	0.11
FeO	23.38	23.46	20.60	17.99	18.47	17.89
MnO	0.33	0.30	0.10	0.07	0.07	0.06
MgO	13.16	13.75	15.55	16.68	16.85	17.77
CaO	0.00	0.01	0.01	0.00	0.00	0.00
ZnO	0.00	0.00	0.08	0.00	0.00	0.05
Na_2O	0.00	0.00	0.00	0.01	0.00	0.00
K_2O	0.00	0.00	0.00	0.00	0.01	0.00
Total	98.47	99.03	99.37	99.52	100.60	100.01
Cations based on 4 oxygens						
Si	0.000	0.000	0.001	0.000	0.000	0.000
Ti	0.000	0.000	0.001	0.000	0.000	0.000
Al	1.943	1.926	1.938	1.965	1.961	1.935
Cr	0.000	0.000	0.001	0.003	0.002	0.002
Fe^{3+}	0.057	0.073	0.058	0.032	0.038	0.063
Fe^{2+}	0.467	0.448	0.392	0.356	0.356	0.320
Mn	0.007	0.007	0.002	0.002	0.001	0.001
Mg	0.525	0.545	0.606	0.642	0.641	0.678
Zn	0.000	0.000	0.002	0.000	0.000	0.001
Ca	0.000	0.000	0.000	0.000	0.000	0.000
Na	0.000	0.000	0.000	0.001	0.000	0.000
K	0.000	0.000	0.000	0.000	0.000	0.000
Total	3.000	3.000	3.000	3.000	3.000	3.000
Mg#	53	55	61	64	64	68
Cr#	0.0	0.0	0.1	0.1	0.1	0.1

Al#	97	96	97	98	98	97
Fe^{3+}#	2.8	3.7	2.9	1.6	1.9	3.1

Mg# =100 Mg / (Mg + Fe^{2+}); Cr# =100 Cr / (Cr + Al); Al# =100 Al / (Cr + Al + Fe^{3+}); Fe^{3+}# =100 Fe^{3+}/ (Cr + $Al+^{Fe3+}$)

* Analysis used for reaction modeling

Table 1c. Representative microprobe analyses of corundum (Crn_1) and clinozoisite (Czo_1).

Sample	S135-25	S135-26	S140-163	S160-14*	S160-105	S135-67	S135-68	S135-69
Mineral	Crn_1	Crn_1	Crn_1	Crn_1	Crn_1	Czo_1	Czo_1	Czo_1
SiO_2	0.10	0.01	0.00	0.00	0.01	39.21	38.94	38.60
TiO_2	0.02	0.00	0.01	0.03	0.02	0.00	0.34	0.00
Al_2O_3	98.55	97.02	97.50	96.73	97.34	31.20	31.21	30.44
Cr_2O_3	0.07	0.17	1.01	1.05	1.74	0.00	0.00	0.18
Fe_2O_3	0.34	0.50	0.18	0.43	0.64	1.92	2.39	2.97
MgO	0.02	0.02	0.00	0.01	0.00	0.03	0.01	0.05
CaO	0.06	0.01	0.00	0.02	0.01	25.12	25.55	25.11
MnO	0.00	0.00	0.03	0.03	0.01	0.10	0.00	0.00
ZnO	0.00	0.00	0.03	0.01	0.04	0.00	0.00	0.00
Na_2O	0.02	0.00	0.01	0.00	0.01	0.01	0.04	0.08
K_2O	0.01	0.00	0.01	0.00	0.00	0.02	0.00	0.00
Total	99.18	97.73	98.79	98.30	99.82	97.61	98.48	97.43
Oxygen Basis	3	3	3	3	3	12.5	12.5	12.5
Si	0.002	0.000	0.000	0.000	0.000	3.010	2.973	2.985
Ti	0.000	0.000	0.000	0.000	0.000	0.000	0.020	0.000
Al	1.991	1.990	1.983	1.979	1.967	2.823	2.809	2.775
Cr	0.001	0.002	0.014	0.014	0.024	0.000	0.000	0.011
Fe^{3+}	0.004	0.007	0.002	0.006	0.008	0.111	0.137	0.173
Mg	0.000	0.000	0.000	0.000	0.000	0.003	0.001	0.006
Ca	0.001	0.000	0.000	0.000	0.000	2.066	2.090	2.081
Mn	0.000	0.000	0.000	0.000	0.000	0.007	0.000	0.000
Zn	0.000	0.000	0.000	0.000	0.000	0.000	0.000	0.000
Na	0.001	0.000	0.000	0.000	0.000	0.001	0.006	0.012
K	0.000	0.000	0.000	0.000	0.000	0.002	0.000	0.000
Cation Σ	2.000	2.000	2.001	2.000	2.000	8.024	8.037	8.042
Pistacite (mole %)						4	5	6

Pistacite (mole %) = 100 Fe^{3+}/ (Fe^{3+}+ Al)

* Analysis used for reaction modeling

Figure 1d. Representative microprobe analyses of plagioclase (Pl) and chlorite (Chl).

Sample	S135-90	S135-95	S135-99	S135-3	S140-130	S160-70*	S140-152
Mineral	Pl	Pl	Pl	Pl	Pl	Pl	Chl
SiO_2	46.27	45.30	45.64	42.35	43.63	43.16	27.70
TiO_2	0.00	0.00	0.00	0.00	0.00	0.00	0.02
Al_2O_3	33.61	33.93	34.05	35.93	34.21	35.53	21.99
Cr_2O_3	0.01	0.02	0.01	0.01	0.00	0.00	0.02
MgO	0.00	0.00	0.00	0.00	0.00	0.00	26.39
FeO	0.10	0.08	0.11	0.08	0.05	0.08	9.05
CaO	18.49	18.74	18.59	20.15	19.95	20.00	0.03
MnO	0.00	0.00	0.00	0.05	0.00	0.00	0.03
ZnO	0.00	0.04	0.02	0.00	0.05	0.00	0.05
Na_2O	1.29	1.05	1.15	0.06	0.40	0.53	0.00
K_2O	0.00	0.00	0.00	0.00	0.00	0.00	0.00
Total	99.77	99.16	99.58	99.39	98.31	99.30	85.27
Oxygen basis	8	8	8	8	8	8	14
Si	2.138	2.109	2.115	1.993	2.058	2.017	2.744
Ti	0.000	0.000	0.000	0.000	0.000	0.000	0.002
Al	1.831	1.862	1.860	1.993	1.902	1.958	2.567
Cr	0.000	0.001	0.000	0.000	0.000	0.000	0.001
Mg	0.000	0.000	0.000	0.000	0.000	0.000	3.896
Fe	0.004	0.003	0.004	0.003	0.002	0.003	0.750
Ca	0.916	0.935	0.923	1.016	1.008	1.001	0.003
Mn	0.000	0.000	0.000	0.002	0.000	0.000	0.002
Zn	0.000	0.001	0.001	0.000	0.002	0.000	0.004
Na	0.116	0.095	0.103	0.006	0.036	0.048	0.000
K	0.000	0.000	0.000	0.000	0.000	0.000	0.000
Cation Σ	5.005	5.007	5.007	5.013	5.009	5.028	9.970
X_{An}	89	91	90	99	97	95	
Mg#							0.84

X_{An} = 100 Ca /(Ca + Na + K); Mg# = Mg / (Mg + Fe^{2+})
* Analysis used for reaction modeling

S140-165 Chl
26.40
0.02
24.75
0.02
24.71
8.98
0.03
0.04
0.01
0.04
0.00
85.01
14
2.620
0.002
2.896
0.002
3.655
0.745
0.004
0.003
0.001
0.008
0.000
9.934
0.83